J. Astrophys. Astr. (2018) 39:15
https://doi.org/10.1007/s12036-017-9502-5

Measurement of coronal properties of Seyfert galaxies from NuSTAR's hard X-ray spectrum

PRIYANKA RANI* and C. S. STALIN

Indian Institute of Astrophysics, Koramangala, Bangalore 560 034, India.
*Corresponding author. E-mail: priyanka@iiap.res.in

MS received 10 September 2017; accepted 17 November 2017; published online 10 February 2018

Abstract. Precise measurement of the coronal properties of Active Galactic Nuclei (AGN) requires the availability of high signal-to-noise ratio data covering a wide range of X-ray energies. The Nuclear Spectroscopic Telescope Array (*NuSTAR*) which is highly sensitive to earlier missions in its operational energy range of 3–79 keV, allows us to arrive at precise estimates of the coronal parameters such as cut-off energy ($E_{\rm cut}$), coronal temperature (kT_e) and geometry of the corona at least for sources that have $E_{\rm cut}$ within the energy range of *NuSTAR*. In this paper, we present our preliminary results on the spectral analysis of two Seyfert galaxies namely 3C 120 and NGC 4151 using *NuSTAR* observations in the 3–79 keV band. We investigated the continuum and coronal parameters, the photon index Γ, $E_{\rm cut}$ and kT_e. By fitting the X-ray spectrum of 3C 120 and NGC 4151 with a simple phenomenological model, we found that both the sources showed a clear cut-off in their spectrum.

Keywords. Galaxies: active—galaxies: Seyfert—galaxies: quasars: individual (3C 120 , NGC 4151).

1. Introduction

Active Galactic Nuclei (AGN) are galaxies that have SuperMassive Black Hole (SMBH) at their centres which accretes material from the galaxies' dense central region. AGN emits copiously over a wide range of the electromagnetic spectrum and they are studied at all accessible wavelengths. Among the various bands, X-ray and γ-ray observations play a vital role in understanding the high energy emission processes happening in the central regions of the AGN. The major components of an AGN include an accretion disk surrounding the central SMBH, an X-ray emitting corona, an obscuring torus surrounding the accretion disk and a relativistic jet in about 15% of AGN (Kellermann *et al.* 1989).The intrinsic X-ray continuum in AGN originates from very near the black hole and thus X-ray spectral and timing studies can provide unique insights into the physical processes occurring close to the central engine. It is believed that the power-law X-ray spectrum in AGN is formed due to the Comptonization process and the shape of this observed spectrum is a function of the seed photon field, the kinetic temperature of the coronal plasma KT_e, the optical depth τ and the geometry of the corona. Therefore, the measurement of the slope of the continuum emission and the high-energy cutoff ($E_{\rm cut}$) in AGN is very important.

In addition to the primary power law continuum, the X-ray spectrum also contains a Fe Kα line at $\sim$6.4 keV as well as a hump around 10–30 keV. The Fe Kα line originates due to the reflection of the power-law photons from the hot corona by the relatively cold accretion disk (George & Fabian 1991) and it was first detected in the source MCG-6-30-15 (Tanaka *et al.* 1995). Several studies have been carried out to find the high energy cut-off using CGRO (Petrucci *et al.* 2001; Marinucci & Tortosa 2016; Lubiński *et al.* 2016; Dadina 2007; Zdziarski *et al.* 2000), *BeppoSAX* (Perola *et al.* 2002) and *INTEGRAL* (Malizia *et al.* 2014). But a large fraction of the $E_{\rm cut}$ measurements available from those missions have large uncertainties.

Using *NuSTAR*, measurements of $E_{\rm cut}$ have been available for about a dozen AGN (Brenneman *et al.* 2014, Baloković *et al.* 2015, Ballantyne *et al.* 2014, Matt *et al.* 2015, Tortosa *et al.* 2016, Kammoun *et al.* 2017, Pahari *et al.* 2017). Though *NuSTAR* observations have enabled us to characterize the coronal properties of about a dozen AGN, precise measurements of the coronal properties for a large sample of AGN are needed to have a complete knowledge of the geometrical and

physical properties of the X-ray corona in AGN. We are in the process of carrying out a systematic investigation of the coronal properties of a large sample of AGN for which *NuSTAR* observations are available. In this paper, we present our preliminary results on two nearby AGN namely 3C 120 and NGC 4151. Detailed results that consider fitting of more physical models to the data on these two sources will be presented elsewhere.

The 3C 120 at a redshift of $z = 0.033$ is a X-ray bright Seyfert 1 galaxy (Burbidge 1967), variable in X-rays (Rani *et al.* 2017) and having a black hole of mass $5.6 \times 10^7 M_\odot$ (Bentz & Katz 2015). Also, classified as a Broad Line Radio Galaxy (BLRG, Walker *et al.* 1987), its radio morphology is similar to the Fanaroff and Riley type I (FRI, Abdo *et al.* 2010) category of AGN (Fanaroff & Riley 1974) with a one-sided jet inclined to the line-of-sight of ∼14° (Eracleous & Halpern 1998). This is based on the apparent superluminal speed $\beta_{\rm app}$ reported by Zensus (1989). The jet has a size of about 100 kpc (Walker *et al.* 1987). The available measurements of $E_{\rm cut}$ are 150^{+230}_{-30} keV from BeppoSAX observations (Zdziarski & Grandi 2001) and 110^{+130}_{-50} keV from ASCA observations (Wozniak *et al.* 1998). A value of $E_{\rm cut}$ of 305^{+142}_{-74} keV was also reported recently by Fabian *et al.* (2017).

The NGC 4151 is a very well-known Seyfert 1 galaxy and it is mostly studied at all wavelengths. It is one of the brightest (bolometric luminosity $\sim 10^{44}$ erg s^{-1}) and nearest Seyfert galaxy at $z = 0.003$. It appears to be in a large barred spiral galaxy seen in optical images with nearly face-on orientation (Arp 1977). Due to heavy absorption, NGC 4151 shows a complex spectrum at soft X-rays. It was previously studied by Beckmann *et al.* 2005 in X-ray wavelength using the *INTEGRAL* (International Gamma-Ray Astrophysics Laboratory) data to get a value of $E_{\rm cut} = 450^{+900}_{-200}$ keV. Using *NuSTAR* observations, Keck *et al.* (2015) reported a value of $E_{\rm cut} = 1000$ keV, which is much beyond the energy coverage of *NuSTAR*, and hence cannot be a true representation of the cutoff in the spectrum of NGC 4151.

It is thus clear that the available $E_{\rm cut}$ measurements for these two sources, 3C 120 and NGC 4151 have large error bars, thereby, necessitating determination of precise values of $E_{\rm cut}$ with better data and/or better models than used before. Therefore, available *NuSTAR* observations on these two sources were looked into for determination of their coronal properties and we give here the preliminary results. More detailed results on these two sources, the analysis of which is currently in progress will be presented elsewhere. The structure of the paper is as follows: In section 2, we describe the *NuSTAR* observations and data reduction. In section 3, we describe the analysis carried out on the data sets. We discuss our results in section 4 and compare our results with earlier measurements in section 5. This is followed by a summary in the last section.

2. Observation and data reduction

In this work, we present our preliminary results on two Seyfert galaxies namely 3C 120 and NGC 4151 observed by *NuSTAR* (Harrison *et al.* 2013) in the 3–79 keV band. The log of observations for both the sources that are used in this study is given in Table 1. The data were reduced using the *NuSTAR* Data Analysis Software package *NuSTARDAS* v1.6.0 distributed by the High Energy Astrophysics Archive Research Center (HEASARC). The cleaned and screened event files were generated using the *nupipeline* task and using CALDB 20161207, and also considering the passage of the satellite through the South Atlantic Anomaly. A circular region of 60″ was taken at the peak of the source image to extract the source spectrum and light curve. To extract the background spectrum and light curve, we selected the same circular region of 60″ away from the source on the same detector. The light curves were generated with 300 s binning in the 3–79 keV band for both the focal plane modules, FPMA and FPMB. To get the final light curves, the count rates from the two modules FPMA and FPMB were combined using the *lcmath* task in FTOOLS v4.0.

For spectral analysis, we generated the source and background spectra in the energy range of 3–79 keV in each of the focal plane modules FPMA and FPMB using the *nuproducts* package available in *NuSTARDAS*. The

Table 1. Log of observations and results of variability analysis in the 3–79 keV band for 3C 120 and NGC 4151.

Name	Type	Obs. ID	Obs. date	Exp. (s)	$F_{\rm var} \pm$ err ($F_{\rm var}$) 3–79 keV
3C 120	Sy 1	60001042003	2013-02-06	127731	0.044 ± 0.003
NGC 4151	Sy 1	60001111002	2012-11-12	21864	0.050 ± 0.002
		60001111003	2012-11-12	57036	0.069 ± 0.003
		60001111005	2012-11-14	61531	0.088 ± 0.002

response matrices were generated using the calibration database (CALDB) version 20161207. In this work, we plotted the spectra for each of the two detectors (FPMA and FPMB) and fitted them simultaneously, allowing cross normalization for both modules to vary freely. In this fitting process, the abundances of elements were fixed to their solar values (Anders & Grevesse 1989). We used *XSPEC* (version 12.9.0; Arnaud 1996) for all spectral analysis. To calculate the errors at 90% significance level, we used the Markov Chain Monte Carlo (MCMC) algorithm available in *XSPEC*.

3. Analysis of the data

3.1 *Flux variability*

To estimate the flux variations if any, shown by the sources, we used the fractional root mean square (rms) variability amplitude ($F_{\rm var}$) which gives an estimate of the intrinsic variability amplitude relative to the mean count rate (Edelson *et al.* 2002; Vaughan *et al.* 2003). Both sources showed variations in the 3–79 keV band as well as in the soft (3–10 keV) and hard (10–79 keV) bands. The results of the variability analysis for both 3C 120 and NGC 4151 in the total 3–79 keV energy band are given in Table 1.

3.2 *Spectral analysis of 3C 120*

Analysis of the spectrum of 3C 120 along with model fittings were carried out using the *XSPEC* package. To find the best-fit models, the χ^2 minimization technique in *XSPEC* was used. We first start the spectral analysis of 3C 120 data by fitting a phenomenological model in which we considered two absorption components, one is for our own galactic absorption and another is for the host galaxy absorption in addition to the continuum. This simple model was first fit to the data to identify the presence of more complex spectral components in the data. The considered model (Model 1) thus has the final form *TBabs* × *zTBabs* × *pow*. In the fitting process, the galactic neutral hydrogen column density was fixed in *TBabs* (Wilms *et al.* 2000) to a value of 1.11×10^{21} cm^{-2} obtained from Dickey and Lockman (1990) using the *nH* tool in HEASARC [1]. The column density in *zTBabs* was kept as a free parameter in the fitting and the redshift was fixed to $z = 0.033$. This gave a poor fit with reduced $\chi^2 = 1.133$ ($\chi^2/\nu = 4299/3795$, where ν is the total degrees of freedom). The best-fit

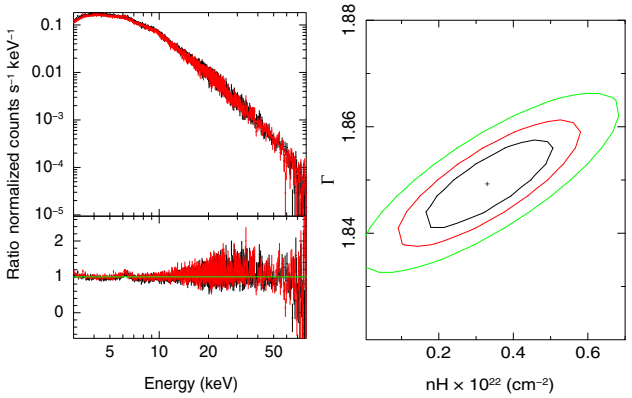

Figure 1. Normalized counts/s against energy (*left panel*) for the source 3C 120. Fits to the data using Model 1 are shown for the modules FPMA (black) and FPMB (red). The data-to-model ratio for both the FPMA (black) and FPMB (red) modules are given in the second panel. The $\Gamma - nH$ contour plot (*right panel*) shows 67% (black), 90% (red) and 99% (green) probability densities. The '+' sign represents the best-fit value of the parameters.

model is shown in Fig. 1 on the top along with residuals. The best-fit parameters of Model 1 are given in Table 2. The residuals of the fit clearly showed a strong signature of the Fe Kα emission line around 6.4 keV which appears because of X-ray reprocessing. There is also an indication of excess emission between 10–35 keV which could be due to Compton up-scattering of accretion disk photons in the corona.

In order to improve our Model 1, we replaced the continuum with an exponential high-energy cutoff power law, the *pexrav* model (Magdziarz & Zdziarski 1995) and added a redshifted Gaussian line (*zgauss*) to fit the excess emission around 6.4 keV. The inclination angle of the reflector was fixed at $\cos i = 0.95$, i.e., $i \approx 17°$, very close to the value of 14° found for the inclination of the jet of the source to the line-of-sight (Eracleous & Halpern 1998) and the abundances of elements were fixed to their solar values (Anders & Grevesse 1989). The observed spectrum with the model fit as well as the residual spectrum are shown in Fig. 2. Model 2 (*TBabs* × *zTbabs* × (*zgauss* + *pexrav*)) gave a better reduced $\chi^2 = 0.999$ ($\chi^2/\nu = 3788/3791$) than Model 1. A model that is more appropriate than *pexrav* is *pexmon* (Nandra *et al.* 2007). For the data sets analysed here, while using $E_{\rm cut}$ as a free parameter, *pexmon* led to unreliable values in the model parameters such as T, etc. Alternatively, *pexrav* model fits to the data led to convergence of the model parameters. Therefore, *pexmon* was not considered in all further analysis. The best-fit parameters of Model 2 are given in Table 2. Using Model 2, we found a $E_{\rm cut}$ value of 83^{+10}_{-8} keV.

[1] https://heasarc.gsfc.nasa.gov/cgi-bin/Tools/w3nh/w3nh.pl.

Table 2. Best-fit parameters and errors (90% confidence) obtained from spectral fitting to the data of 3C 120 for two different models. Here, $N_{\rm H}$ is the hydrogen column density, Γ is the photon index, E and σ are the peak energy and width of the Fe Kα line, $E_{\rm cut}$ is the cut-off energy, R is the reflection fraction and $N_{\rm pow}$ and N_{pexrav} are the normalizations in the model fits to the data.

Model name	Parameter name (units)	Parameter values	χ^2/dof
Model 1			
TBabs × *zTBabs* × *pow*	$N_{\rm H}$ (10^{22}cm^{-2})	0.33 ± 0.11	1.133
	Γ	1.85 ± 0.01	
	$N_{\rm pow} \times 10^{-2}$	1.67 ± 0.04	
Model 2			
TBabs × *zTBabs* × (*zgauss* + *pexrav*)	E (keV)	6.45 ± 0.05	0.999
	σ (keV)	$0.15^{+0.10}_{-0.12}$	
	$N_{zgauss} \times 10^{-5}$	$3.34^{+0.76}_{-0.70}$	
	Γ	1.87 ± 0.02	
	$E_{\rm cut}$ (keV)	83^{+10}_{-8}	
	R	0.55 ± 0.07	
	$N_{pexrav} \times 10^{-2}$	1.73 ± 0.04	

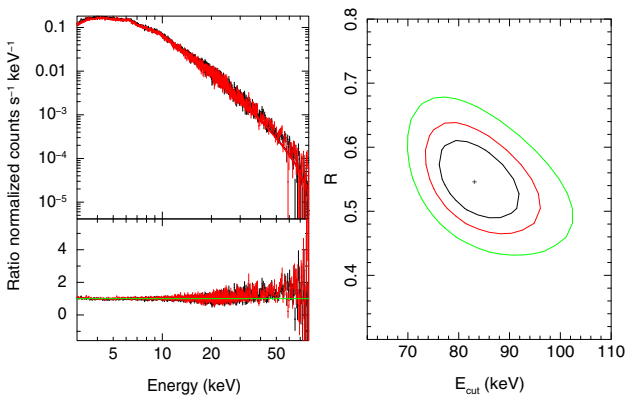

Figure 2. *Left panel:* Normalized counts/s versus energy for the model *TBabs* × *zTBabs*(*zgauss* + *pexrav*) for the source 3C 120. Here, black and red refer to FPMA and FPMB modules respectively. This plot also gives the ratio of data-to-model for the FPMA (black) and FPMB (red) modules. *Right panel:* Contour plot of $R - E_{\rm cut}$ using MCMC analysis. Here, the black, red and green contours refer to the 67%, 90% and 99% confidence levels respectively, and the '+' sign represents the best-fit value of the parameter.

3.3 *Spectral analysis of NGC 4151*

We have three epochs of observations from *NuSTAR* for NGC 4151 as mentioned in Table 1. Here too, similar to 3C 120, first we fit the spectra with the simple phenomenological model, Model 1. In the fitting process, the galactic neutral hydrogen column density of *TBabs* component was frozen to the value of 2.30×10^{20} cm^{-2} obtained from Kalberla *et al.* (2005) and the redshift was fixed to $z = 0.003$ in *zTBabs*. This fit yielded a poor reduced χ^2 for observational IDs 60001111002, 60001111003 and 60001111005 with values of 1.29 ($\chi^2/\nu = 4897/3795$), 1.86 ($\chi^2/\nu = 7268/3795$) and 1.92 ($\chi^2/\nu = 7268/3795$) respectively. The best-fit model is shown in Fig. 3 on the top along with residuals. The residuals of the fit in Fig. 3 clearly showed strong signatures of the Fe Kα emission line around 6.3 keV. This indicated the inadequacy of Model 1 to fit the data of NGC 4151. To improve the fitting, we added a Gaussian line to Model 1. The new model (Model 2) has the form *TBabs* × *zTBabs* × (*zgauss* + *pexrav*). The spectra along with model-fit are shown in Fig. 4. During the fit using Model 2, the abundances of elements were fixed to their solar values (Anders & Grevesse 1989) and the inclination angle of the reflector was fixed at its default value of $\cos i = 0.45$, i.e., $i \approx 60°$. The fit improved significantly for all the three epochs of observations. We obtained $E_{\rm cut}$ values of 59 ± 4, 64 ± 3 and 70 ± 3 keV for the observational IDs 60001111002, 60001111003 and 60001111005 respectively. The best-fit parameters are shown in Table 3.

4. Comparison of results

4.1 *3C 120*

Good quality data for a single epoch spanning about 120 ks was available from *NuSTAR* for 3C 120. It is

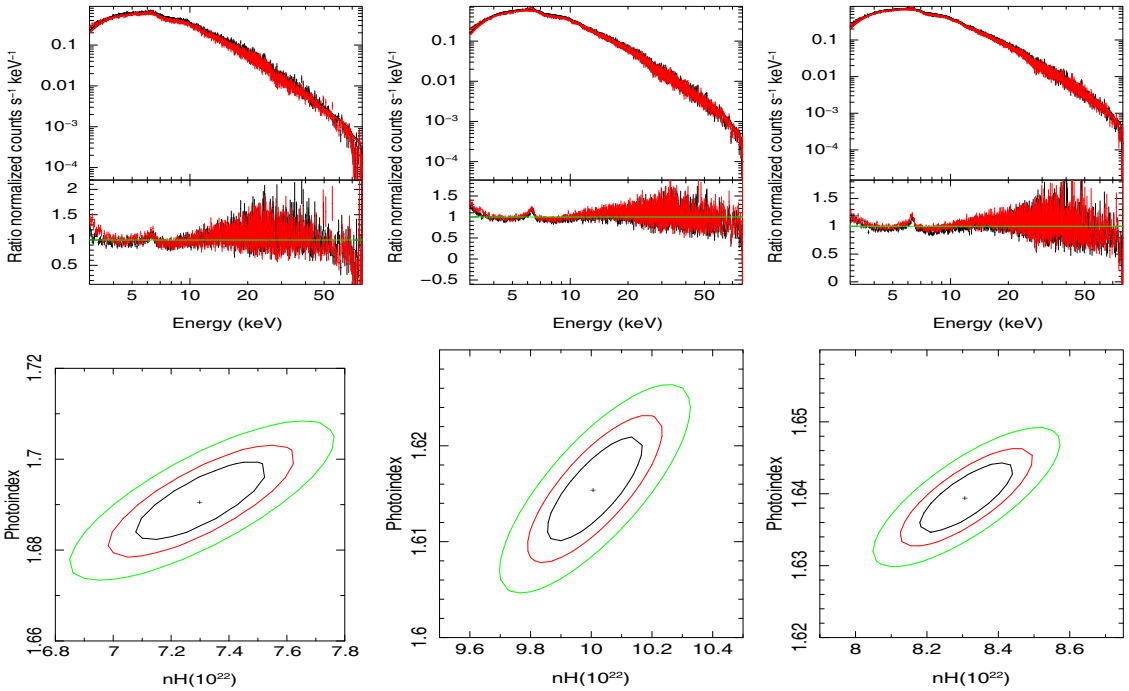

Figure 3. Model fits to the data for NGC 4151. The normalized counts/s against energy (*upper panels*) for the model *TBabs* × *zTBabs* × *pow* are shown separately for the FPMA (black) and FPMB (red) for Obs ID 60001111002, 60001111003 and 60001111005 respectively. The data-to-model ratio for both the FPMA (black) and FPMB (red) modules are given in the second panel. The $\Gamma - nH$ contour plot (*bottom panels*) shows 67% (black), 90% (red) and 99% (green) probability densities. The '+' sign represents the best-fit values of the parameters.

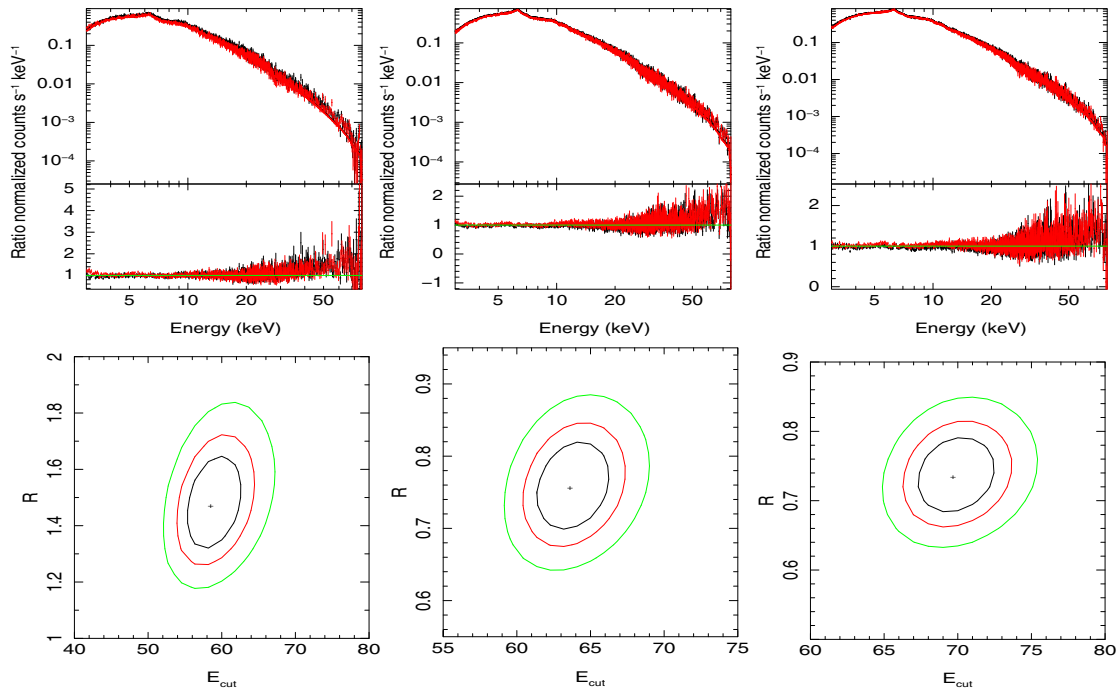

Figure 4. Model fits to the data for NGC 4151. The normalized counts/s against energy (*upper panels*) for the model *TBabs* × *zTBabs*(*zgauss* + *pexrav*) are shown separately for the FPMA (black) and FPMB (red) for Obs ID 60001111002, 60001111003 and 60001111005 respectively. The data-to-model ratio for both the FPMA (black) and FPMB (red) modules are given in the second panel. The $R - E_{\rm cut}$ contour plot (*bottom panels*) shows 67% (black), 90% (red) and 99% (green) probability densities. The '+' sign represents the best-fit values of the parameters.

Table 3. Best-fit parameters and errors (90% confidence) of NGC 4151 obtained from spectral fitting of the *NuSTAR* data using two different models. The notations have the same meaning as that of Table 2.

NGC 4151	Obs. ID	Parameter name (units)	Parameter values	χ^2/dof
Model 1	60001111002	$N_{\rm H}$ ($10^{22}{\rm cm}^{-2}$)	7.30 ± 0.14	1.29
TBabs × *zTBabs* × *pow*		Γ	1.69 ± 0.005	
		$N_{\rm pow} \times 10^{-2}$	6.51 ± 0.02	
	60001111003	$N_{\rm H}$ ($10^{22}{\rm cm}^{-2}$)	10.01 ± 0.10	1.86
		Γ	1.61 ± 0.003	
		$N_{\rm pow} \times 10^{-2}$	5.60 ± 0.01	
	60001111005	$N_{\rm H}$ ($10^{22}{\rm cm}^{-2}$)	8.31 ± 0.08	1.92
		Γ	1.64 ± 0.003	
		$N_{\rm pow} \times 10^{-2}$	6.62 ± 0.01	
Model 2	60001111002	E (keV)	6.26 ± 0.05	0.94
TBabs × *zTBabs* × (*zgauss* + *pexrav*)		σ (keV)	0.19 ± 0.06	
		Γ	1.66 ± 0.03	
		$E_{\rm cut}$ (keV)	59 ± 4	
		R	$1.47^{+0.07}_{-0.06}$	
		$N_{pexrav} \times 10^{-2}$	5.16 ± 0.2	
	60001111003	E (keV)	6.25 ± 0.02	1.12
		σ (keV)	0.23 ± 0.03	
		Γ	1.46 ± 0.02	
		$E_{\rm cut}$ (keV)	64 ± 3	
		R	$0.76^{+0.07}_{-0.06}$	
		$N_{pexrav} \times 10^{-2}$	3.58 ± 0.09	
	60001111005	E (keV)	6.26 ± 0.02	1.12
		σ (keV)	0.20 ± 0.004	
		Γ	1.51 ± 0.02	
		$E_{\rm cut}$ (keV)	70 ± 3	
		R	0.74 ± 0.06	
		$N_{pexrav} \times 10^{-2}$	4.60 ± 0.1	

classified as a Seyfert 1 galaxy (Burbidge 1967) and as well as a BLRG (Walker *et al.* 1987). It has a one-sided jet and is also detected in γ-rays by *Fermi* (Sahakyan *et al.* 2015). By fitting Model 2 (*TBabs* × *zTBabs* × (*zgauss* + *pexrav*)) to the data, we obtained best-fit values of $E_{\rm cut} = 83^{+10}_{-8}$ keV and $\Gamma = 1.87 \pm 0.02$. This value of Γ obtained here is comparable to earlier estimates of Γ available in literature as well as the recent estimate of $\Gamma = 1.70^{+0.10}_{-0.03}$ by Fabian *et al.* (2017). The 3C 120 is a radio-loud AGN, and therefore in comparison to NGC 4151 (the other Seyfert 1 galaxy studied in this work), the jet in 3C 120 might play a significant role in shaping its overall spectral properties. The value of Γ obtained for 3C 120 from spectral fits in this work, is similar to the typical photon indices known for Seyfert galaxies. We hence, argue for negligible contribution of the jet emission to the X-ray data from *NuSTAR* that is analysed here. The value of $E_{\rm cut} = 80^{+10}_{-8}$ obtained here for 3C 120 is lower compared to the values already available in literature. It matches within 2σ to that reported by Zdziarski & Grandi (2001) and Wozniak *et al.* (1998), however, it does not agree with the high value reported by Fabian *et al.* (2017). The values of $E_{\rm cut}$ and Γ obtained in this work have much lower uncertainties compared to the measurements that were already available in literature.

4.2 *NGC 4151*

Three sets of observations were available for NGC 4151 from *NuSTAR* with exposure times ranging from about 20–60 ks. All the three data sets were best-fit with Model 2 (*TBabs* × *zTBabs* × (*zgauss* + *pexrav*)) compared to Model 1 (*TBabs* × *zTBabs* × *pow*). Our model fits to the three sets of observations gave values of $E_{\rm cut}$ of 59 ± 4, 64 ± 3 and 70 ± 3 keV. They agree within 1σ of each other. This is also very much evident in the observed spectra shown in Figures 3 and 4 where a curvature is noticeable beyond 50 keV. These new measurements with smaller error bars are lower than

the value of $E_{\rm cut} = 450^{+900}_{-200}$ keV from *INTEGRAL*, however, within error bars to that reported by Petrucci *et al.* (2001) and Rosa *et al.* (2007). Keck *et al.* (2015) too have analysed *NuSTAR* data of NGC 4151, wherein they have fixed an $E_{\rm cut}$ value of 1000 keV in all their spectral fittings and thus the $E_{\rm cut}$ values obtained in this work cannot be directly compared with that of Keck *et al.* (2015). Fitting of Model 2 to the data yielded Γ values of 1.66 ± 0.03, 1.46 ± 0.02 and 1.51 ± 0.02. This clearly indicates that NGC 4151 showed spectral variability between the epochs of *NuSTAR* observations.

5. Summary

We have carried out timing and spectral analysis of *NuSTAR* observations on the Seyfert 1 galaxies 3C 120 and NGC 4151. The results of our preliminary analysis are summarized below:

(1) Both the sources showed flux variations in the 3–79 keV band. Among the two, NGC 4151 showed larger $F_{\rm var}$ in all the three epochs of observations relative to 3C 120 for which only one epoch of *NuSTAR* data was available. For 3C 120, we obtained a photon index $\Gamma = 1.87 \pm 0.02$, whereas for NGC 4151, we derived values of $\Gamma = 1.66 \pm 0.03$, 1.46 ± 0.02 and 1.51 ± 0.02 for the three epochs of observations.
(2) For both the sources, the *TBabs* × *zTBabs* × *pow* model provided a bad fit to the data. The residuals of the simple phenomenological model fit to the data sets of 3C 120 and NGC 4151 indicated the presence of the Fe Kα emission line. Also, excess emission was seen beyond 10 keV which is due to Compton reflection of X-ray photons by the accretion disk.
(3) The fit to the data of 3C 120 gave a value of $E = 6.45 \pm 0.05$ keV and $\sigma = 0.15^{+0.10}_{-0.12}$ keV for the Fe Kα line. For NGC 4151, the Fe Kα is present at 6.26 ± 0.05 keV. It is well fit by a Gaussian with a σ of about 0.19 $\pm$ 0.06 keV.
(4) Using phenomenological model fits to the data of 3C 120, we find a high energy cut-off $E_{\rm cut} = 83^{+10}_{-8}$ keV and a reflection fraction of $R = 0.55 \pm 0.07$. For NGC 4151, we find $E_{\rm cut}$ values of 59 ± 4, 64 ± 3 and 70 $\pm$ 3 keV for the three epochs of observations. Though they match within 2σ of each other, using the present data it would not be possible to make any firm statement on the change of $E_{\rm cut}$ between different epochs of observations for NGC 4151. The $E_{\rm cut}$ values obtained here on these two sources are much better, with drastic reduction in their errors, than those already available in the literature.

Acknowledgements

The first author, PR thanks the organizers of the National Conference on Recent Trends in the Study of Compact Objects – Theory and Observation (RETCO-III) for providing the opportunity to participate in the meeting and give a presentation of the preliminary results. The authors also thank the referee for his/her critical and valuable comments that improved the paper significantly.

References

Abdo, A. A. *et al.* 2010, ApJ, 720, 912
Anders, E., Grevesse, N. 1989, Geochim. Cosmochim. Acta, 53, 197
Arnaud, K. A. 1996, in Jacoby, G. H., Barnes, J., eds, Astronomical Society of the Pacific Conference Series, Vol. 101, Astronomical Data Analysis Software and Systems V, p. 17
Arp, H. 1977, ApJ, 218, 70
Ballantyne, D. R. *et al.* 2014, ApJ, 794, 62
Baloković, M. *et al.* 2015, ApJ, 800, 62
Beckmann, V., Shrader, C. R., Gehrels, N., Soldi, S., Lubiński, P., Zdziarski, A. A., Petrucci, P.-O., Malzac, J. 2005, ApJ, 634, 939
Bentz, M. C., Katz, S. 2015, PASP, 127, 67
Brenneman, L. W. *et al.* 2014, ApJ, 781, 83
Burbidge, E. M. 1967, ApJ, 149, L51
Dadina, M. 2007, A&A, 461, 1209
de Rosa, A., Piro, L., Perola, G. C., Capalbi, M., Cappi, M., Grandi, P., Maraschi, L., Petrucci, P. O. 2007, A&A, 463, 903
Dickey, J. M., Lockman, F. J. 1990, ARA&A, 28, 215
Edelson, R., Turner, T. J., Pounds, K., Vaughan, S., Markowitz, A., Marshall, H., Dobbie, P., Warwick, R. 2002, ApJ, 568, 610
Eracleous, M., Halpern, J. P. 1998, ApJ, 505, 577
Fabian, A. C., Lohfink, A., Belmont, R., Malzac, J., Coppi, P. 2017, MNRAS, 467, 2566
Fanaroff, B. L., Riley, J. M. 1974, MNRAS, 167, 31P
George, I. M., Fabian, A. C. 1991, MNRAS, 249, 352
Harrison, F. A. *et al.* 2013, ApJ, 770, 103
Kalberla, P. M. W., Burton, W. B., Hartmann, D., Arnal, E. M., Bajaja, E., Morras, R., Pöppel, W. G. L. 2005, A&A, 440, 775
Kammoun, E. S. *et al.* 2017, MNRAS, 465, 1665
Keck, M. L. *et al.* 2015, ApJ, 806, 149
Kellermann, K. I., Sramek, R., Schmidt, M., Shaffer, D. B., Green, R. 1989, AJ, 98, 1195
Lubiński, P. *et al.* 2016, MNRAS, 458, 2454
Magdziarz, P., Zdziarski, A. A. 1995, MNRAS, 273, 837
Malizia, A., Molina, M., Bassani, L., Stephen, J. B., Bazzano, A., Ubertini, P., Bird, A. J. 2014, ApJ, 782, L25

Marinucci, A., Tortosa, A. 2016, NuSTAR AGN Physics Working Group 2016, Astron. Nachr., 337, 490
Matt, G. *et al.* 2015, MNRAS, 447, 3029
Nandra, K., O'Neill, P. M., George, I. M., Reeves, J. N. 2007, MNRAS, 382, 194
Pahari, M., McHardy, I. M., Mallick, L., Dewangan, G. C., Misra, R. 2017, preprint, arXiv:1706.02489
Perola, G. C., Matt, G., Cappi, M., Fiore, F., Guainazzi, M., Maraschi, L., Petrucci, P. O., Piro, L. 2002, A&A, 389, 802
Petrucci, P. O. *et al.* 2001, ApJ, 556, 716
Rani, P., Stalin, C. S., Rakshit, S. 2017, MNRAS, 466, 3309
Sahakyan, N., Zargaryan, D., Baghmanyan, V. 2015, A&A, 574, A88
Tanaka, Y. *et al.* 1995, Nature, 375, 659
Tortosa, A. *et al.* 2016, preprint, arXiv:1612:05871
Vaughan, S., Edelson, R., Warwick, R. S., Uttley, P. 2003, MNRAS, 345, 1271
Walker, R. C., Benson, J. M., Unwin, S. C. 1987, ApJ, 316, 546
Wilms, J., Allen, A., McCray, R. 2000, ApJ, 542, 914
Wozniak, P. R., Zdziarski, A. A., Smith, D., Madejski, G. M., Johnson, W. N. 1998, MNRAS, 299, 449
Zdziarski, A. A., Grandi, P. 2001, ApJ, 551, 186
Zdziarski, A. A., Poutanen, J., Johnson, W. N. 2000, ApJ, 542, 703
Zensus, J. A. 1989, in Maraschi, L., Maccacaro, T., Ulrich, M.-H., eds, Lecture Notes in Physics, Berlin Springer, vol. 334, BL Lac Objects, p. 3, https://doi.org/10.1007/BFb0031137